

# Supporting Information

## Single-step soft-imprinted large-area nanopatterned anti-reflection coating

*Jorik van de Groep,<sup>1</sup> Pierpaolo Spinelli,<sup>1,2</sup> and Albert Polman<sup>\*,1</sup>*

<sup>1</sup> Center for Nanophotonics, FOM Institute AMOLF, Science Park 104, 1098 XG Amsterdam, The Netherlands

<sup>2</sup> Energy Research Center of the Netherlands ECN, Westerduinweg 3, 1755 LE Petten, The Netherlands

### AUTHOR INFORMATION

#### **Corresponding Author**

\*polman@amolf.nl

## S1. Ellipsometry on silica solgel

Spectroscopic ellipsometry was used to determine the optical constants of the silica-based solgel. A Si wafer was spin coated with a 90 nm thick layer of solgel (800 rpm, 10s) and left to dry for 30 minutes in ambient conditions. A Cauchy model was used as a model in the ellipsometry analysis. The real part of the refractive index for  $400 \leq \lambda \leq 1100$  nm ranged from  $n = 1.448$  to  $n = 1.432$  (Fig. S1). The imaginary part of the index ( $\kappa$ ) is found to be smaller than 0.005, by comparing calculated ellipsometry data with the experimental data, taking into account the measurement errors.

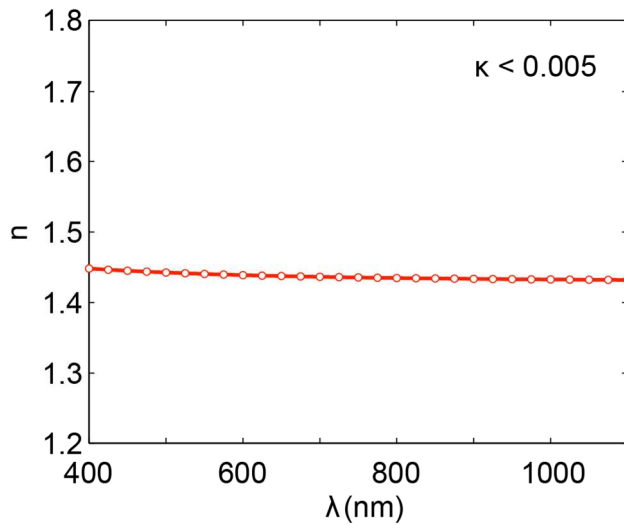


**Figure S1.** Real part of the refractive index obtained from spectroscopic ellipsometry. The imaginary part of the refractive index  $\kappa$  is smaller than 0.005 over the entire spectral range.

## S2. Integrating sphere measurement procedure

Figure S2 illustrates a top view of the experimental procedure used to measure the total reflection spectra reported in Fig. 2a. The incoming light is an attenuated white-light supercontinuum laser (Fianium SC400-4). The light enters the integrating sphere

(LabSphere, 4") through the entrance port and travels through the sphere unperturbed. An 8° mount at the exit port is used to mount the samples and reference sample systematically with an 8° angle of incidence, to prevent the specularly reflected light to escape back out of the entrance port. The inside of the sphere is coated with white scattering powder (Spectralon) such that the specularly reflected light is randomized and trapped inside the sphere, until it is collected at the collection port (at the top of the sphere).

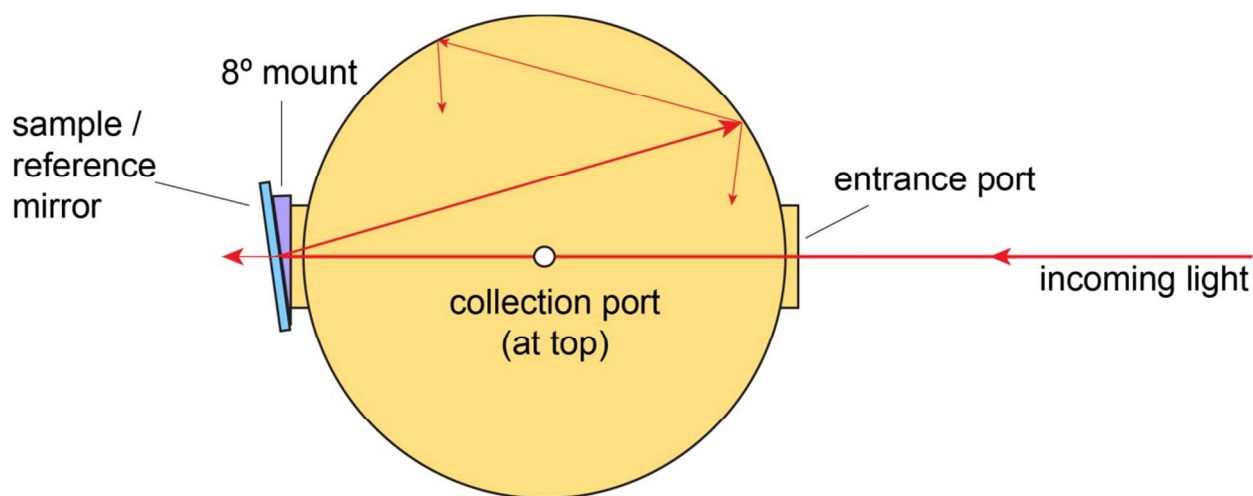


**Figure S2.** Schematic (top view) of integrating sphere setup used to measure the total reflection spectra reported in Fig. 2a.

To accurately determine the reflection spectrum of a sample, the spectrum measured on the sample ( $I_{sample}$ ) has to be compared to the spectrum measured on a reference sample with 100% reflection ( $I_{100\%}$ ), such that the system response of the light source, optics, sphere, collection fiber, spectrograph and CCD camera can be eliminated:

$$R_{sample} = \frac{I_{sample}}{I_{100\%}}$$

In our experiments, we used a protected silver mirror (Thorlabs, PF10-03-P01) as reference sample. To take into account the non-perfect reflectance of the mirror in the reference measurement ( $I_{mirror}$ ), we use the reflectance spectrum specified by the supplier ( $R_{mirror}$ ) to correct for the non-perfect reflection of the mirror:

$$R_{sample} = \frac{I_{sample}}{I_{100\%}} = \frac{I_{sample}}{I_{mirror}} R_{mirror}$$

The mirror spectrum can be obtained from the supplier's website:

[http://www.thorlabs.de/images/TabImages/Thorlabs\\_Protected\\_Silver\\_Coating.xlsx](http://www.thorlabs.de/images/TabImages/Thorlabs_Protected_Silver_Coating.xlsx)

### S3. FDTD simulations

To further corroborate that the nanopattern AR coating functions as an effective medium, as well as to demonstrate the coupling to guided substrate modes in the blue spectral range, we performed finite-difference time-domain (FDTD) simulations of light reflecting off the top interface using Lumerical Solutions.<sup>1</sup> A constant refractive index of  $n = 1.44$  is used for the solgel nanoparticles ( $d = 245$  nm, 325 nm pitch) and the 30 nm residual layer, and the substrate is assumed to be semi-infinite ( $n_{sub} = 1.485$ ). A broad-band plane wave ( $\lambda = 400 - 1000$  nm) is used as a source from the top with normal incidence. Periodic boundary conditions and a 2.5 nm refinement mesh are used.

Figure S3a shows the real part of the electric field (top) and its phase (bottom) for light with  $\lambda = 600$  nm propagating through the nanopatterned layer. Both the field and the phase front clearly demonstrate that the light propagates through the nanoparticle array as an unperturbed plane-wave, thereby showing that the nanopattern AR coating functions as an effective medium for  $\lambda = 600$  nm.

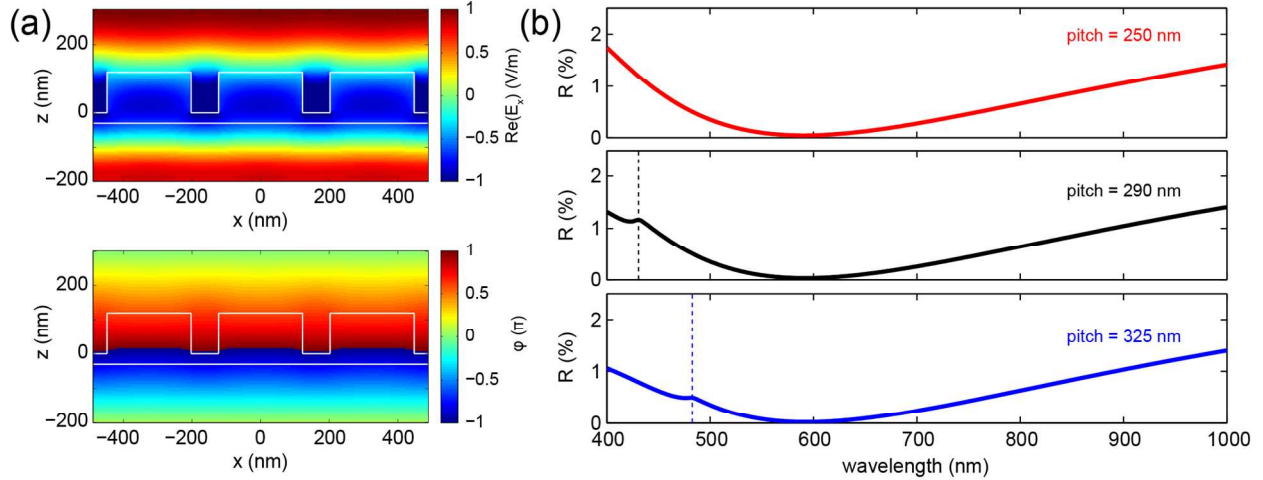


**Figure S3.** (a) Simulated real part of the electric field (top) and its phase (bottom) for  $\lambda = 600$  nm showing flat phase fronts after propagation through the nanopattern AR coating. (b) Simulated reflection spectra for top interface with different nanoparticle pitch (constant effective index  $n_{eff} = 1.196$ ).

To demonstrate that diffractive coupling to guided modes occurs in the blue spectral range we compare the simulated reflectance spectra for different nanoparticle array pitch while keeping the effective index of the nanoparticle coating constant ( $n_{eff} = 1.196$ ). Figure S3b shows the reflection spectra for 250 nm (top, red), 290 nm (black, middle), and 325 nm pitch (blue, bottom) used in the experiments. The nanoparticle height is 120 nm for all pitches, and the particle diameter is 188.5 nm, 218.6 nm and 245 nm respectively. The vertical dashed lines indicate the calculated maximum wavelength for which diffractive coupling occurs under normal incidence. Note that these simulations only consider the top interface, such that the diffracted light is not coupled back out. As a result, diffractive coupling to guided substrate modes is observed as a reduction in reflectance rather than an increase. Figure S3b demonstrates that: first, the spectral range where mode coupling occurs shifts with pitch, as expected for diffractive coupling, and

second, mode coupling in the visible spectral range can be eliminated by reducing the pitch to 250 nm.

Final proof for the diffraction of light in the blue spectral range can be obtained from the power scattered into the diffracted orders, as calculated using Lumerical's far-field transformation routine.<sup>1</sup> The total field (all  $E$  and  $H$  components) is simulated 50 nm below the interface. A far-field projection, taking into account the periodicity of the structure, is then used to calculate which fraction of the transmitted light is coupled to the different diffraction orders. For  $\lambda \geq 483$  nm, all transmitted light is coupled to the 0<sup>th</sup> order (normal) transmission. However, for  $\lambda < 483$  nm light couples to the  $\pm 1$  diffraction orders. For example, at  $\lambda = 430$  nm the total calculated transmittance into the substrate is 99.2%, of which 5.6% is coupled to the  $\pm 1$  diffraction orders and 93.6% to the 0<sup>th</sup> diffractive order. The 5.6% of the incoming light can subsequently couple back out and thereby contribute the experimentally measured reflection.

#### **S4. Haze**

Haze, or diffuse scattering is an undesired property for optical coatings with potential applications in display applications. Haze reduces the visibility and readability of the underlying display as a result of uncontrolled random scattering. The nanopattern AR coating shown in this work is designed to have limited or even no scattering (see Fig. S3a), and should therefore exhibit extremely low haze levels. To demonstrate this, Fig. S4 shows a photograph of the AMOLF logo imaged through flat (left), one-side (center) and two-side (right) coated substrates. Applying the coating clearly improves the readability of the text as a result of reduced reflection of outdoor light, while no scattering is visible (i.e. extremely low haze).

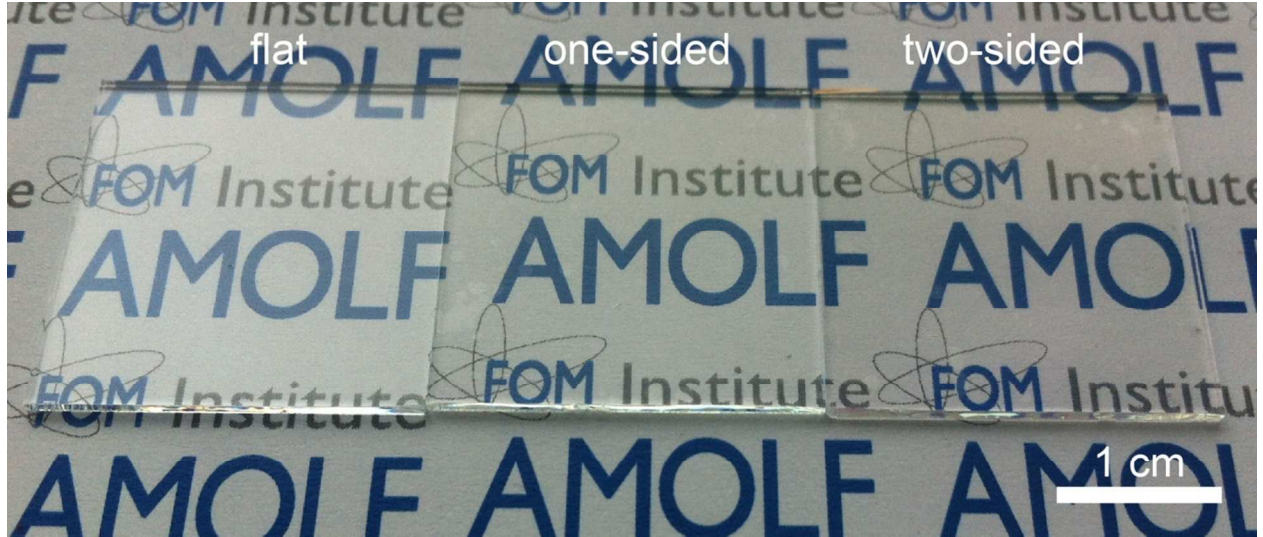


**Figure S4.** Photograph of text imaged through flat (left), one-side (center) and two-side (right) coated substrates.

### **S5. Polarization-controlled specular reflection measurements**

Figure S5 shows the measured angle-resolved specular reflectance for s- (open symbols) and p-polarized (closed symbols) light for a flat (blue), one-side coated (red) and double-side coated (black) substrate ( $\lambda = 532$  nm, 325 nm pitch). A significantly higher reflectance is observed for s-polarized light for all substrates as expected. For both s- and p-polarized light, the AR coating strongly reduces the reflectance over the entire angular range. A small drop in reflection is observed at  $\theta = 39.5^\circ$  for s-polarized light; it is less pronounced for p-polarized light, indicating that s-polarized light couples more efficiently to the guided modes in the substrate.

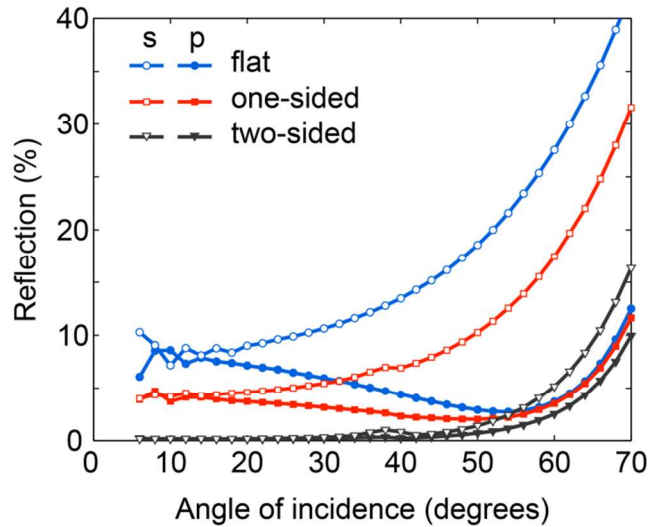


**Figure S5.** Measured specular reflection ( $\lambda = 532$  nm) for a flat (blue), one side coated (red) and double-side coated substrate (black). Open symbols show the reflection for s-polarized light, closed symbols for p-polarized light.

### S6. Dispersion calculations of diffracted orders

Figure S6a shows the calculated dispersion curves for the  $0^{\text{th}}$  (red) and  $\pm 1^{\text{st}}$  (blue) grating orders ( $G = 2\pi/p$ ) as a function of angle of incidence, upon scattering from the nanopatterned interface ( $\lambda = 532$  nm,  $p = 325$  nm). A continuum of guided modes lies between the light line in air and in the substrate ( $n = 1.485$ , shaded regions) because the substrate is thick (1 mm). Mode coupling occurs for the  $-1^{\text{st}}$  diffraction order that crosses the continuum of (backward propagating) modes for  $8.5^\circ < \theta < 39.5^\circ$ . The coupling mechanism is schematically illustrated in Fig. S3b.



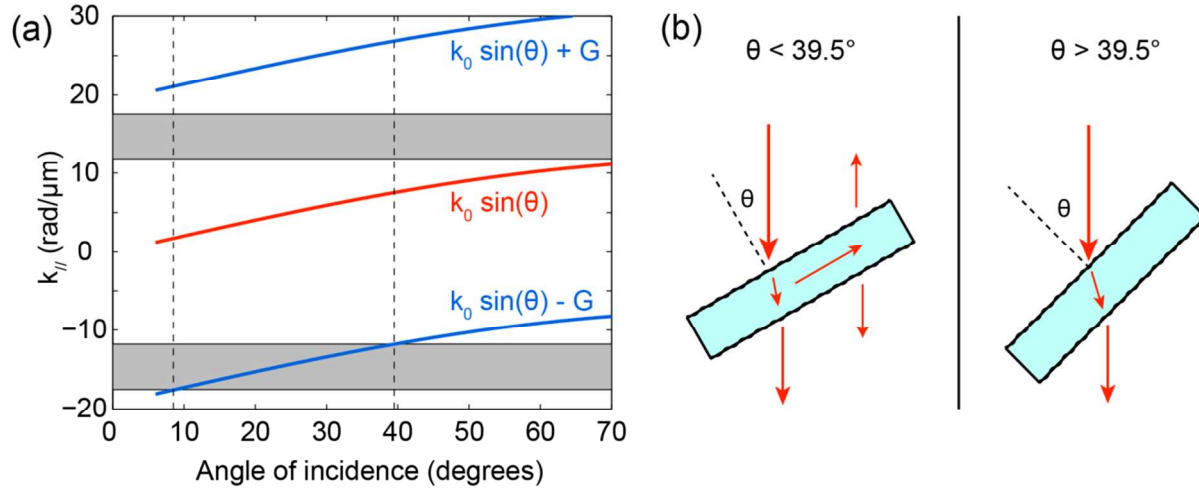


**Figure S6.** (a) Calculated dispersion curves for  $\lambda = 532$  nm and  $p = 325$  nm, showing coupling to guided modes occurs for  $8.5^\circ < \theta < 39.5^\circ$ . The continuum of guided modes is indicated by the shaded areas. (b) Schematic indicating the mode coupling mechanism for  $\theta < 39.5^\circ$  and lack of mode coupling for  $\theta > 39.5^\circ$ .

### S7. Duct tape stripping

To study the mechanical rigidity of the nanopattern AR coating, we applied, pressed and removed both office tape and vinyl duct tape (3M 3903i) onto the patterned surface. Figure S7 shows SEM images (FEI Verios, 2 kV, 100 pA) of the sample after tape removal. Clear lines of residual adhesive are visible. However, the underlying nanopattern is undamaged (see insets).

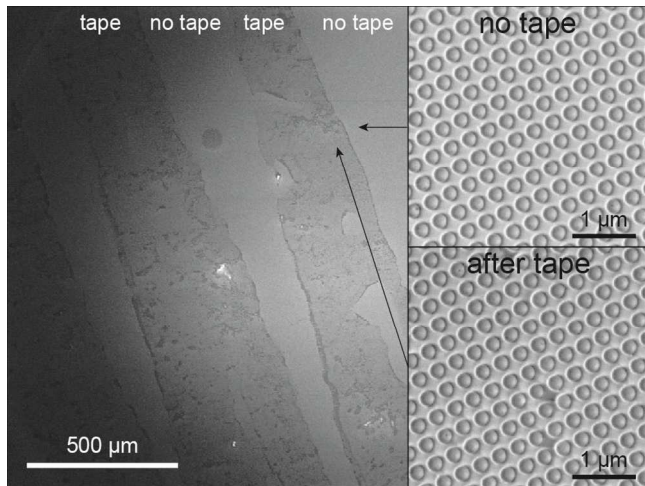


**Figure S7.** SEM image of nanopattern AR coating after duct tape removal. The insets show large-magnification SEM images of both regions exposed (bottom) and unexposed (top) to the tape adhesive.

## REFERENCES

1. Lumerical Solutions Inc. [www.lumerical.com](http://www.lumerical.com).